JOURNAL OF NEUROPHYSIOLOGY
Vol. 74, No. 6, December 1995. *Printed in U.S.A.*

Nonlinear Models of the First Synapse in the Light-Adapted Fly Retina

M. JUUSOLA, M. WECKSTRÖM, R. O. UUSITALO, M. J. KORENBERG, AND A. S. FRENCH
Department of Physiology and Biophysics, Dalhousie University, Halifax, Nova Scotia B3H 4H7, Canada; Department of Physiology, University of Oulu, Oulu, Finland; and Department of Electrical Engineering, Queen's University, Kingston, Ontario K7L 3N6, Canada

SUMMARY AND CONCLUSIONS

1. Randomly modulated light stimuli were used to characterize the nonlinear dynamic properties of the synapse between photoreceptors and large monopolar neurons (LMC) in the fly retina. Membrane potential fluctuations produced by constant variance contrast stimuli were recorded at eight different levels of background light intensity.

2. Representation of the photoreceptor-LMC input-output data in the form of traditional characteristic curves indicated that synaptic gain was reduced by light adaptation. However, this representation did not include the time-dependent properties of the synaptic function, which are known to be nonlinear. Therefore nonlinear systems analysis was used to characterize the synapse.

3. The responses of photoreceptors and LMCs to random light fluctuations were characterized by second-order Volterra series, with kernel estimation by the parallel cascade method. Photoreceptor responses were approximately linear, but LMC responses were clearly nonlinear.

4. Synaptic input-output relationships were measured by passing the light stimuli to LMCs through the measured photoreceptor characteristics to obtain an estimate of the synaptic input. The resulting nonlinear synaptic functions were well characterized by second-order Volterra series. They could not be modeled by a linear-nonlinear-linear cascade but were better approximated by a nonlinear-linear-nonlinear cascade.

5. These results support two possible structural models of the synapse, the first having two parallel paths for signal flow between the photoreceptor and LMC, and the second having two distinct nonlinear operations, occurring before and after chemical transmission.

6. The two models were each used to calculate the synaptic gain to a brief change in photoreceptor membrane potential. Both models predicted that synaptic gain is reduced by light adaptation.

INTRODUCTION

The first synapse in the arthropod compound eye occurs between the axons of the photoreceptor cells and a group of second-order neurons, the large monopolar cells (LMCs). These synapses are located in a layer named the Lamina ganglionaris. There is always a convergence of several photoreceptors onto a group of Lamina cells, but in the diptera (flies) there is a special optical and physical arrangement called neural superposition (van Hateren 1987; Kirschfeld 1967), in which photoreceptors from different facets, but having similar optical orientations, send processes laterally to converge on the second-order neurons.

The synaptic transmitter between photoreceptors and LMCs is histamine (Hardie 1989). The release of histamine is continuous, even under dark-adapted conditions (Juusola et al. 1995; Laughlin and Osorio 1989; Uusitalo et al. 1995a; Weckström et al. 1989). Histamine opens chloride-permeable channels in the LMC membrane. In the most commonly recorded neurons, types L1 and L2, the equilibrium potential for chloride is approximately −90 mV, compared with a resting membrane potential of approximately −40 mV, so that transmitter release hyperpolarizes the membrane. Therefore changes in membrane potential of LMCs and photoreceptors are normally of opposite polarity (Dubs 1981; Järvilehto and Zettler 1970; Shaw 1968). The synapse amplifies, so that responses to light flashes are larger in LMCs than in photoreceptors. It also gives an adaptive filtering. At low light backgrounds, LMC contrast responses are low-pass filtered, but with increasing light adaptation, higher frequencies are amplified more, and the response becomes bandpass (van Hateren 1992; Juusola et al. 1995; Srinivasan et al. 1990).

Systems analysis techniques have been applied to photoreceptors of diptera in several previous investigations (Eckert and Bishop 1975; French 1980a,b; French and Järvilehto 1978; Gemperlein and McCann 1975; Juusola et al. 1994, 1995; Marmarelis and McCann 1977; Weckström et al. 1988). Although there are detectable nonlinearities, particularly under dark-adapted conditions (French et al. 1993; Juusola 1993; Weckström et al. 1995), light-adapted photoreceptors are approximately linear when subjected to random contrast fluctuations (Juusola et al. 1994). However, even with bright backgrounds, LMC behavior is clearly nonlinear, because light fluctuations evoke asymmetric responses (French and Järvilehto 1978; Juusola et al. 1995; Laughlin et al. 1987; Uusitalo et al. 1995b). Several mechanisms could be involved in these nonlinearities, including voltage-activated conductances in the photoreceptor axon or LMC membranes, nonlinear dependence of transmitter release on membrane potential, synaptic feedback from neighboring LMC or amacrine cells, cooperativity or inactivation of histamine receptors, changes in chloride equilibrium potential, or voltage effects from the extracelluar space, which is known to generate significant potential changes.

Although it is not yet possible to record simultaneously from a photoreceptor and a synaptically connected LMC, recordings from photoreceptors are so well characterized, stable, and reliable, that it is possible to measure the photoreceptor response separately and then use this to predict the synaptic input to an LMC. This approach was used pre-

viously to measure the linear frequency response function of the synapse (French and Järvilehto 1978; Juusola et al. 1995). Here we used the same approach to estimate the actual membrane potential fluctuations in the photoreceptors that were causing the measured LMC response. These input-output data were used to construct and test several simple nonlinear models of synaptic function. Two models that gave reliable predictions of synaptic signal transfer were then used to calculate the synaptic impulse response, a function that has never been measured experimentally, and that is important for understanding the mechanisms of synaptic transmission.

METHODS

Animals and stimulation

Flies, *Calliphora vicina,* were obtained from a laboratory culture. Adults and larvae were fed on liver, yeast, and sucrose, and the stock was refreshed regularly with wild flies. Each fly was attached with beeswax onto a platform with a rotating Cardan arm, and a silver chloride reference electrode was mounted near the retina inside the head. Ventilation was maintained by leaving the abdomen intact with spiracles functioning normally. All experiments were performed at room temperature (21–23°C).

Light stimuli were provided by a green light-emitting diode (LED; Stanley HBG5666X, with peak emission at 555 nm) subtending <2° at the eye surface. The LED was driven by a linearized voltage to current converter (Juusola et al. 1994). The linearity of the light source was checked by both radiometer and linearized photodiode detectors. Computer-generated pseudorandomly modulated stimuli were superimposed on a steady light background. The contrast (c) of the pseudorandom stimuli was defined as

$$c = \frac{\Delta I}{I_{mean}} \tag{1}$$

where ΔI was the standard deviation of the intensity modulation and I_{mean} was the mean background (see Juusola et al. 1994). The pseudorandom stimuli were Gaussian, having a flat power spectrum up to ~250 Hz, and the contrast value, c, in *Eq. 1* was 0.32. Light outputs of >5 log units were attenuated by neutral density filters (Kodak Wratten) to provide eight different adapting backgrounds. Each experiment proceeded from the weakest to the strongest adapting background. After stimulation, cells were re-dark adapted. Recordings were rejected if the same sensitivity was not recovered by dark adaptation.

Recording procedures

Before recordings, the cells were allowed to light adapt for 2 min. Borosilicate glass microelectrodes, filled with 1.5 M potassium acetate and 2.5 mM potassium chloride, had resistances of 80–250 MΩ. Electrodes were mounted on a piezoelectric microtranslator (Burleigh PZ-550 inchworm controller) and entered the compound eye through a small lateral hole in the cornea that was sealed with high vacuum grease. Membrane potentials were recorded with an intracellular amplifier (SEC-10L, NPI Electronic, Germany) operating in the balanced bridge mode. Recordings were made from R1–6 photoreceptors and LMCs. In photoreceptor somata recordings, the correct retinal recording site was indicated by frequent successive microelectrode penetrations of photoreceptors, and the negative-going electroretinogram (ERG) detected by the same electrode between penetrations. Lamina penetration was verified by a depolarizing ERG and by the alternating impalements of photoreceptor axons and LMCs as the electrode was advanced through the tissue.

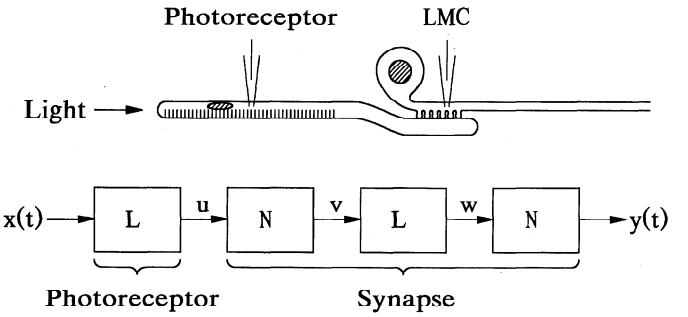

FIG. 1. Nonlinear cascade model of synaptic transmission. *Top*: fly photoreceptor and its synapse with a large monopolar cell (LMC). Pseudorandomly varying light stimuli were presented to 1 facet of the eye while recording from a stimulated photoreceptor or LMC in the regions shown. *Bottom*: NLN cascade model of the synapse. The input light signal, $x(t)$, 1st passed through a linear dynamic filter (L) representing phototransduction. The synapse was represented by a cascade of nonlinear static (N), linear dynamic (L), and nonlinear static elements (N) to give the membrane potential in the LMC membrane.

Responses were filtered at 500 Hz, together with the corresponding LED current signals, by a VBF/23 low-pass, dual-channel, elliptic filter (KEMO). Both signals were monitored by an oscilloscope, sampled at 1 kHz, digitized by a 12-bit A/D converter (DT2821, Data Translation), and stored on a computer disk. The sampling was synchronized to the computer-generated stimulus signal, and 8.192-s records of both signals were stored during each recording cycle. After a preset number of responses (10–30) the average response was calculated (see also French 1980b).

Data analysis

Input-output relationships for photoreceptors, photoreceptor-LMC combinations, and photoreceptor-LMC synapses were initially modeled by Volterra series of the form

$$y(t) = k_0 + \sum_{\tau=0}^{T} k_1(\tau)x(t-\tau) + \sum_{\tau_1=0}^{T}\sum_{\tau_2=0}^{T} k_2(\tau_1,\tau_2)x(t-\tau_1)x(t-\tau_2) \tag{2}$$

where $x(t)$ and $y(t)$ were the input and output signals as functions of time, t, and k_0, $k_1(\tau)$, $k_2(\tau_1, \tau_2)$ were the zero-, first-, and symmetrical second-order kernels, respectively. The system memory was assumed to last until a maximum lag of T. The kernels were estimated by the parallel cascade method (Korenberg 1982, 1991) with the use of second-order polynomial functions. The kernels obtained were very nearly least-squares estimates, and because a Gaussian input was used, k_1 and k_2 were estimates of the first- and second-order Wiener kernels, respectively. A total of 8,192 data pairs (input and output) were obtained from each experiment. The 1st 8,000 data pairs were used for estimation of the kernels. The remaining 192 were used as independent data to predict the output of the Volterra series and to measure the quality of its prediction via the percentage mean square error (MSE)

$$MSE = 100\,\frac{\overline{(y-y')^2}}{\bar{y}^2 - \bar{y}^2}, \tag{3}$$

where y was the actual system output, y' was the model estimate of the output, and the bars indicate mean values.

To check the measured kernels, independent estimates were obtained from the same data by the fast orthogonal algorithm (Korenberg 1988; Korenberg et al. 1988). Kernels obtained by this algorithm were similar in form, but less smooth than the parallel cascade kernels. All of the data presented here were obtained by the parallel cascade method.

The nonlinear cascade structure used to fit the photoreceptor-LMC synapse is shown in Fig. 1. The input signal, $x(t)$, measured

the contrast of the light stimulus as a function of time, t. The first component of the cascade, representing the photoreceptor, was a linear dynamic system (L)

$$u(t) = \sum_{\tau=0}^{T} g(\tau)x(t-\tau) \quad (4)$$

where $g(t)$ was the impulse response of the photoreceptor. The synaptic function between the photoreceptor and LMC membrane potential signals (u, y, respectively) was a cascade of nonlinear static (N), linear dynamic (L), and nonlinear static (N) components. The linear dynamic component had the same form as *Eq. 4*, but with a distinct impulse response function, $h(t)$. The nonlinear static components were represented by fourth-order polynomials. For example, the second nonlinear static component, N, was represented by

$$y(t) = c_0 + c_1 w(t) + c_2 w(t)^2 + c_3 w(t)^3 + c_4 w(t)^4 \quad (5)$$

where c_n are the coefficients.

The impulse response of the first linear system, $g(t)$, corresponding to the photoreceptor was obtained directly from the first-order kernel, k_1, of the Volterra series (*Eq. 2*). The nonlinear dynamic properties of the synapse were then obtained from LMC recordings by first passing the appropriate input light stimulus signal through the convolution (*Eq. 4*) to give the synaptic input. The convolution used the impulse response, $g(t)$ obtained in a separate experiment at the corresponding background level (see RESULTS). The nonlinear cascade model of the synapse was then fitted to the synapse input-output data with the use of the Levenberg-Marquardt general nonlinear technique (Press et al. 1990) to minimize the MSE (*Eq. 3*). To obtain an initial estimate of the impulse response function, $h(\tau)$, of the linear system in the cascade, the synaptic input-output data were first fitted by a second-order Volterra series. The initial estimates of the polynomials were linear functions of unity gain. Fitting was performed on the 1st 2,000 data pairs from each experiment, and the algorithm always converged successfully. Prediction of the model output and final MSE measurements were made with the use of a 2nd set of 2,000 points, which had not been used for fitting.

RESULTS

Photoreceptor and LMC recordings were obtained at eight different background light levels (BL1 to BL8) corresponding to light intensities of 160, 500, 1,600, 5,000, 16,000, 50,000, 160,000, and 500,000 effective photons per second in a typical photoreceptor. All of the data presented here were obtained from single, high-quality recordings of one photoreceptor cell and one LMC. This approach has been used before to examine nonlinearities in dark adapted photoreceptors (French et al. 1993) and to detect small nonlinearities in light-adapted photoreceptors (Weckström et al. 1995).

Synaptic characteristic curve

The photoreceptor-LMC synaptic function has often been represented by a characteristic curve that relates the peak membrane potential responses in LMCs and photoreceptors to the same step light stimulus (e.g., Laughlin et al. 1987). To create a similar plot from our data, the digitized values of both photoreceptor and LMC responses to a period of random light fluctuation were first sorted by amplitude. The justifications for sorting were that the distribution of responses to Gaussian noise stimulation had a single maximum, and the known monotonic, sigmoidal relationship between photoreceptor and LMC responses (Juusola et al. 1995). Figure 2 shows the light-adaptational shift in the characteristic curves obtained by plotting the sorted photoreceptor response amplitude distributions, scaled around their means on the x-axis, versus the corresponding LMC distributions on the y-axis. It can be seen that both the photoreceptor and LMC responses increased with light adaptation, but the synaptic gain (the slopes of the characteristic curves) decreased with light adaptation.

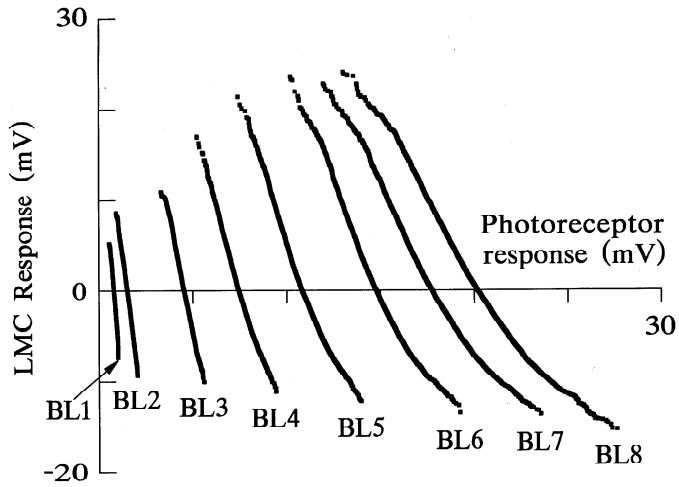

FIG. 2. Synaptic characteristic curves at 8 different background light levels. Curves were calculated from photoreceptor and LMC responses to a random noise stimulus with Gaussian contrast distribution. The digitized pre-and postsynaptic response amplitude distributions were sorted by amplitude and scaled around the mean values. Note how both the photoreceptor and LMC responses increased, the synaptic gain decreased (i.e., the slope of the curves), and the mean photoreceptor potential rose, with increasing light adaptation.

A characteristic curve plot cannot give an accurate measure of synaptic gain because of the time-dependent properties of the visual cells, which have a significant effect on contrast step responses, and the adaptation-dependent delay in signal transfer through the synapse. This becomes obvious at high adapting backgrounds, where photoreceptors responses have much slower integration times than the corresponding LMC responses (Juusola 1993; Juusola et al. 1994, 1995). For example, positive contrast steps at background level BL8 in blowfly photoreceptors must exceed 8 ms to give the maximum photoreceptor response, whereas a stimulus duration of 2–3 ms is sufficient for LMC responses to reach their maximum. Therefore, with increasing contrast steps, as the LMC responses peak before the photoreceptor responses, gain estimation based on maximum responses becomes unreliable and dependent on the selected stimulus duration. The measurements of Fig. 2 used the Gaussian distributions of the stimulus and responses to try to overcome these problems, but the adaptation-dependent synaptic delay was still a limitation, and more detailed models of synaptic function are necessary. The remainder of this work attempts to provide such models.

Photoreceptor responses

The photoreceptor responses to white noise–modulated stimuli were continuously changing depolarizations and hyperpolarizations, as described before (e.g., Juusola et al.

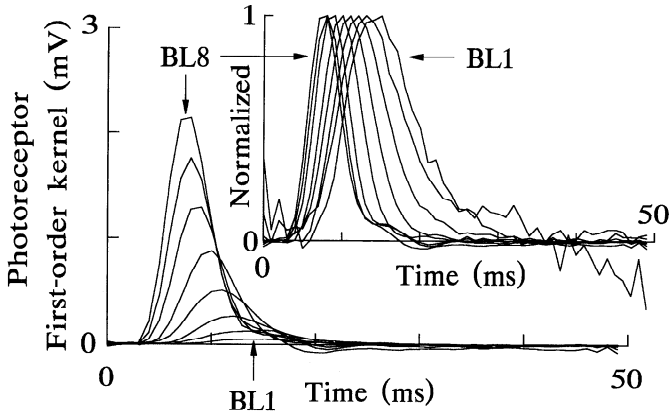

FIG. 3. First-order kernels (linear impulse responses) between light input and membrane potential of fly photoreceptors at 8 different background levels. Responses increased in amplitude and became faster at increasing background levels. Normalized responses (*inset*) illustrate the changing time course and decreasing inherent noise with background level.

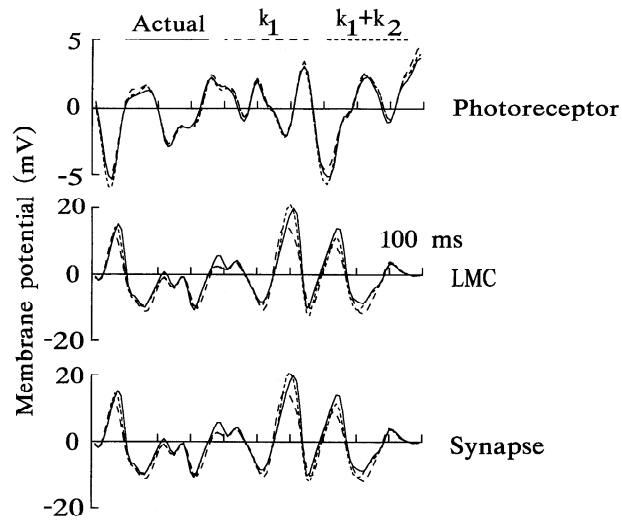

FIG. 4. Actual and predicted membrane potential fluctuations in photoreceptors and LMCs during pseudorandom contrast stimulation at background level BL8. *Bottom figure* shows the LMC output predicted by modeling the photoreceptor as a linear dynamic system. Each set of traces shows the actual signal and the predictions from *Eq. 2* using k_1 alone, and both k_1 and k_2.

1994). First- and second-order kernels of photoreceptor responses had similar forms to those reported previously from linear and nonlinear examinations of fly eyes (Eckert and Bishop 1975; French 1980a,b; French and Järvilehto 1978; Gemperlein and McCann 1975; James 1992; Juusola et al. 1994, 1995; Marmarelis and McCann 1977; Weckström et al. 1988). First-order kernels at the eight different background levels (Fig. 3) showed typical delayed onsets and increasing speed as the background level increased. The amplitudes of the first-order kernels increased with background level because the constant contrast amplitudes corresponded to increasing numbers of photons per unit contrast. Second-order kernels (not shown) were relatively small.

Table 1 shows the percentage MSE values indicating the goodness-of-fit of the modeling, obtained by synthesizing the output from the resulting first- and second-order kernels (*Eq. 2*). At low background levels the inherent noise level of the recordings was so great, even after averaging, that the MSE levels were high. The residual inherent noise can also be seen in the normalized kernels of Fig. 3. However, the noise level improved with increasing light adaptation, so that MSE values <10% were seen at background levels BL5–BL8. Table 1 also shows that the second-order kernels made insignificant contributions to the photoreceptor responses,

TABLE 1. *Percentage MSE between the Volterra series model and actual photoreceptor output signals at 8 different mean background levels*

Background Level	k_1	$k_1 + k_2$
BL1	127.0	134.7
BL2	79.2	76.2
BL3	112.2	109.6
BL4	15.5	15.8
BL5	7.0	4.8
BL6	3.4	5.7
BL7	2.8	2.2
BL8	2.7	1.8

Note that addition of the 2nd-order kernel did not significantly improve the quality of the fit to the data. In this and subsequent tables, the MSE was measured on test data not used to estimate the kernels. MSE, mean square error.

with the MSE between actual and predicted photoreceptor responses being essentially unchanged by addition of the second-order kernel to the model. This is further illustrated in Fig. 4, which shows the final 50 ms of output data from a photoreceptor at BL8, together with predictions based on the same input data, the first-order kernel alone, and the combined first- and second-order kernels. Addition of the second-order kernel did not visibly improve the prediction. This analysis supports previous findings of linear photoreceptor responses obtained with white noise stimulation (Juusola et al. 1994; Weckström et al. 1988). On this basis, we were able to model the photoreceptor as a linear filter and use the calculated photoreceptor output as the input to the synapse (see also Juusola et al. 1995).

LMC responses

White noise stimulation also elicited a continuously fluctuating membrane potential in the postsynaptic elements of the fly compound eye, the large monopolar cells, or LMCs. Figure 5 shows first-order kernels for the LMC responses at eight different background levels, both in absolute units and when normalized to constant peak amplitude. LMC responses were inverted and larger than the corresponding photoreceptor responses to the same stimulus amplitude, as shown previously (Juusola et al. 1995; Laughlin et al. 1987). LMC responses increased in amplitude and speed with increasing background levels. They also showed significant late positive overshoots at background levels BL4–BL8.

In contrast to the photoreceptors, LMC behavior was clearly nonlinear. This caused the MSE values of Table 2, which were higher than the corresponding photoreceptor values at higher background levels, indicating that a linear prediction could not satisfactorily explain the recorded responses. This was also seen in the records of Fig. 4.

For LMCs, addition of the second-order kernel improved the MSE and the appearance of the prediction (Fig. 4). The

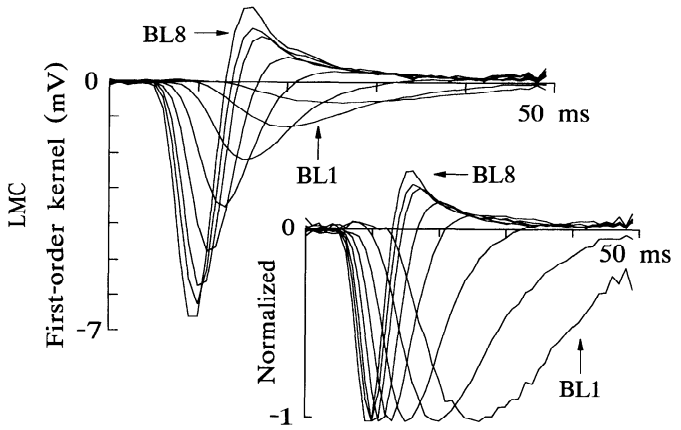

FIG. 5. First-order kernels between light input and LMC membrane potential responses at 8 different background levels. Responses were larger than in photoreceptors. They increased in amplitude and became faster and more overshooting as the background level was increased. Normalized responses (*inset*) also show the increased speed, overshoot, and decreased noise.

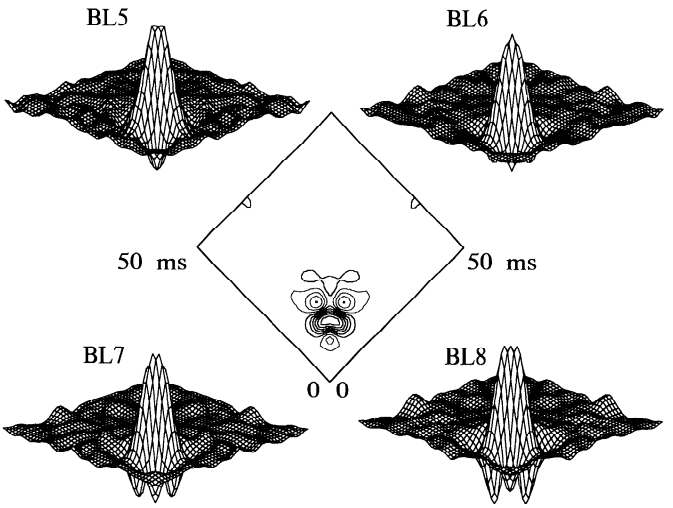

FIG. 6. Second-order kernels between light input and LMC membrane potential responses at the 4 brightest background levels. The *4 outer figures* show perspective plots. All the kernels gave a nonlinear reduction of the response at short times (<10 ms) followed by a stronger nonlinear enhancement. At higher background levels there was an increasing off-axis nonlinear reduction of the response. The center plot is a contour map of the 2nd-order kernel at BL8 to show the time course of the kernels. Contours were drawn at 10% intervals of the total range. All kernels are shown after 1 smoothing, total amplitude ranges of the unsmoothed kernels were 5.5, 7.58, 9.52, and 6.61 mV^2 for levels BL5–BL8, respectively.

improvement in MSE could only be seen at levels BL5–BL8 because of the inherent noise at lower background levels. Because of the relatively high noise levels at BL1–BL4, the remaining figures only present data from levels BL5–BL8, where MSE values were <10% for all model fitting. The second-order kernels obtained from the LMC responses (Fig. 6) had three major features: an early diminution of the response on the diagonal at ~8 ms, a stronger enhancement on the diagonal at ~11 ms, and a further, off-diagonal diminution at ~12 ms, 17 ms.

Synaptic function

As outlined in METHODS, the input-output relationships for the synapse were obtained by convolving the input stimuli that were used for LMC measurements with the first-order kernels of the photoreceptor measurements at the same background levels, which was justified by the very linear behavior of the photoreceptor responses. This gave new data sets representing the synaptic input signals. These input signals were then used, together with the corresponding LMC outputs, to measure the kernels as above. The first- and second-order kernels for the synapse are shown over a total lag duration of 25 ms, rather than 50 ms, because of their more rapid time courses.

TABLE 2. *Percentage MSE between model and actual LMC output signals at 8 different mean background levels*

Background Level	k_1	$k_1 + k_2$
BL1	46.3	45.13
BL2	19.3	17.3
BL3	10.0	10.5
BL4	8.4	5.3
BL5	9.6	4.6
BL6	13.0	4.7
BL7	14.4	5.4
BL8	16.3	6.0

Note the improvement in fit produced by the 2nd-order kernel at high background levels. MSE, mean square error; LMC, large monopolar cell.

First-order kernels of the synapse for levels BL5–BL8 are shown in Fig. 7. These kernels were much faster than for the LMCs, because LMC responses are normally dominated by the slow responses of the photoreceptors. The amplitude of the synaptic response decreased with increasing background level, in contrast to the increasing responses seen in the photoreceptors and LMCs. This decreased gain of the synapse has been reported before (Juusola et al. 1995). The time course of the synaptic response at the four highest background levels was largely unchanged (normalized responses, *inset* Fig. 7), especially during the 1st 5 ms. After this, there was a smaller and more rapid damped oscillation at higher background levels. At the three lowest backgrounds (not shown) the time course of the synaptic response was slower but became faster with increasing light background, as described before for the synaptic transfer delay (Juusola et al. 1995, Fig. 9*C*).

The synaptic second-order kernels also had an approxi-

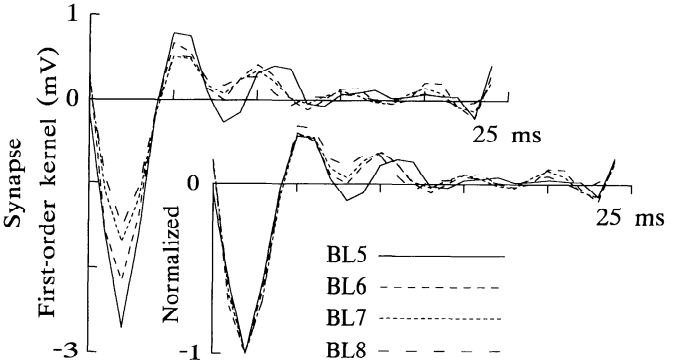

FIG. 7. First-order kernels of the photoreceptor-LMC synapse at levels BL5–BL8. Note the similarity in the normalized shapes of the kernels (*inset*) and the reduced amplitude with increasing background level.

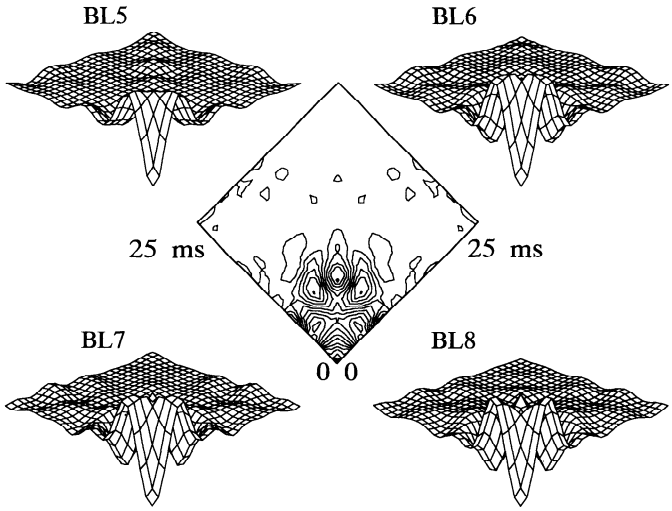

FIG. 8. Second-order kernels of the synapse at levels BL5–BL8. Kernels are shown as perspective plots with a 10% contour map of level BL8 (*middle*). Note that the kernels have similar forms to each other and are much faster than the corresponding LMC kernels. All kernels are shown after 1 smoothing. Total amplitude ranges of the unsmoothed kernels were 0.31, 0.13, 0.086, and 0.068 mV^2 for levels BL5–BL8, respectively.

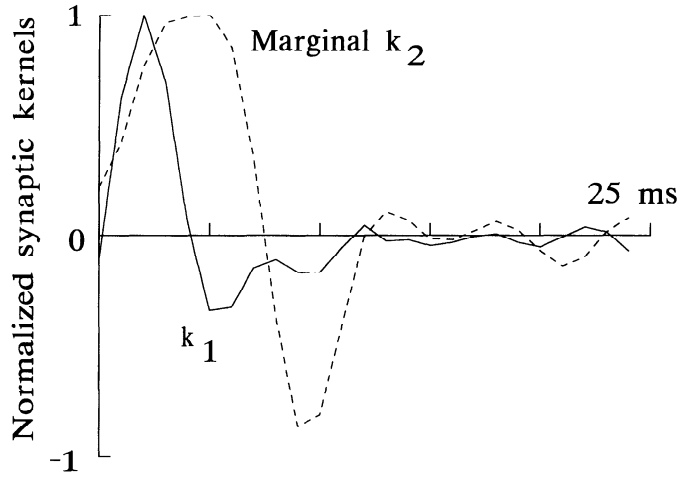

FIG. 9. Test of the ability of an LNL cascade model to fit the synaptic input-output data. For this type of cascade, the marginal kernel obtained by collapsing the 2nd-order Wiener kernel along 1 time axis (*Eq. 6*) should be proportional to the 1st-order Wiener kernel. The test failed for synaptic data, as shown here for level BL8.

mately constant form with changing background level (Fig. 8), although in this case they increased in amplitude with background level. The second-order kernels were also more rapid, starting with a nonlinear diminution of the response at the shortest intervals then proceeding through several positive and negative peaks with considerable off-axis spread. The nonlinear character of the synapse is additionally illustrated by the improved MSE values (Table 3) and the visible improvement on addition of the second-order kernel to the prediction (Fig. 4).

Nonlinear cascade model

Several simple nonlinear cascade models have been used previously in attempts to account for the nonlinear dynamic properties of real physiological systems. These cascade models are constructed from components that are either linear dynamic functions (L) or nonlinear static functions (N). The simplest cascade models are the Wiener (LN) and Hammerstein (NL) models (Hunter and Korenberg 1986; Korenberg 1973; Marmarelis and Marmarelis 1978). A further elaboration of these are the sandwich models, either LNL or NLN, which both have the Wiener and Hammerstein models as substructures. The LNL model has been used successfully to model sensory transduction in an insect mechanoreceptor (French and Korenberg 1989; Korenberg et al. 1988), whereas the NLN model has been applied to the nonlinearities observed with very large step changes in light input to fly photoreceptors (French et al. 1993). The LNL model is more tractable because it is possible to calculate the parameters of the cascade components from the first- and second-order kernels and the experimental record.

A simple test is available to determine whether the LNL model can be applied to a nonlinear system (Chen et al. 1986; Korenberg 1973; Korenberg and Hunter 1986). If second-order, or other Wiener kernels of order n are integrated along $n - 1$ lag axes, then the resulting functions should be proportional to the first-order Wiener kernel. This function has been called the marginal integral (James 1992). For the discrete time second-order Wiener kernel, this corresponds to

$$k(\tau_1) = C \sum_{\tau_2=0}^{T} k_2(\tau_1,\tau_2) \qquad (6)$$

where C is a constant.

Figure 9 shows the results of this test for the first- and second-order Wiener kernels of the synapse at level BL8. For this, and other synaptic kernels, the marginal kernel was clearly not proportional to the first-order kernel, so that a LNL cascade model cannot be used to model the synapse.

There are no such simple tests for the alternative, NLN model (Fig. 1), and, although it may have a significantly smaller number of parameters if low-order polynomials are used, these parameters cannot readily be calculated directly from low-order Wiener kernels. As before (French et al. 1993), we fitted NLN models to the synaptic input-output data with the use of a nonlinear fitting algorithm to vary each parameter in turn, while searching for the minimum MSE. The two polynomials were initially set to be linear with unit slope, and the linear function had an impulse func-

TABLE 3. *Percentage MSE between model and actual outputs of the photoreceptor-LMC synapse at 8 different mean background levels*

Background Level	k_1	$k_1 + k_2$	NLN Model
BL1	74.9	74.1	53.1
BL2	33.5	33.2	26.5
BL3	31.8	33.2	13.0
BL4	15.5	9.4	9.0
BL5	16.9	7.7	5.9
BL6	15.1	5.3	7.3
BL7	14.9	5.0	7.7
BL8	18.1	8.5	9.6

NLN model, a sandwich model consisting of nonlinear static functions (N) and linear dynamic functions (L); for other abbreviations, see Table 2.

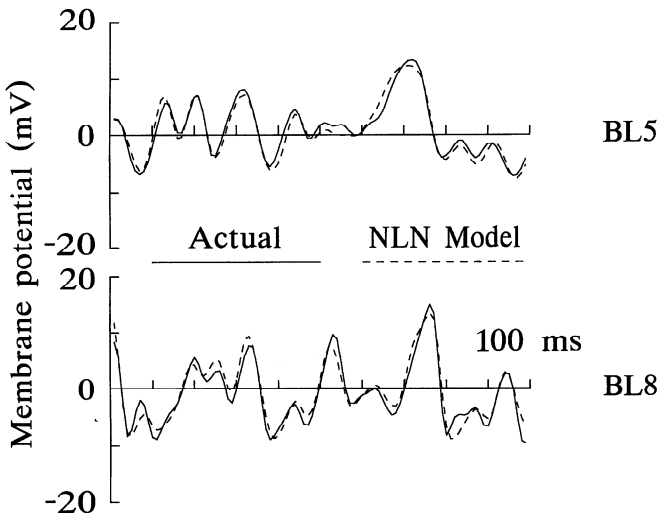

FIG. 10. Actual membrane potential fluctuations in LMC cells at levels BL5 and BL8 during white noise stimulation, together with the predicted outputs of the NLN cascade model to the same input signals.

tion, $h(\tau)$, that was initially set to be identical to the first-order kernel.

Table 3 shows that the NLN model was capable of predicting the synaptic output with MSE below 10% at the five highest background levels. The MSE levels were comparable with those obtained from the combined first- and second-order kernels. The agreement between the predicted and actual outputs was also satisfactory (Fig. 10).

The forms of the components of the NLN cascade model were reliable at the different background levels. Figure 11 shows the first nonlinear static component, central linear dynamic component, and final nonlinear static component, for the highest four background levels. The dimensions of the parameters in these functions cannot be reliably stated unless they can be correlated with physical components, although the abscissa of the first nonlinear static component is photoreceptor membrane potential (mV), and the ordinate of the second nonlinear static component is LMC membrane potential (mV). For simplicity, all of the axes of the nonlinear static components have been labeled in millivolts, so that $h(\tau)$ is dimensionless.

Synaptic impulse response

The responses of the synapse to brief changes in photoreceptor membrane potential were calculated from the NLN model and also from the combined first- and second-order kernels. The amplitudes of these responses are shown in Fig. 12 as functions of background level and input pulse amplitude. This function would be difficult to measure experimentally but is important for producing an accurate physical model of synaptic transmission and modulation. The impulse responses from the two nonlinear models both showed a decreasing synaptic gain with increasing background light level. For 5-mV hyperpolarizations of the photoreceptor membrane, the gain decreased from ~4.8 to ~2.3 as the background increased from BL5 to BL8 for the NLN model and from ~2.7 to ~1.5 for the kernel model. The NLN model gain was more obviously nonlinear as a function of impulse amplitude, predicting much smaller gains from 2-mV depolarizations of the photoreceptor membrane (~2.5 to ~1.4 for levels BL5 to BL8). The reasons for the reduction in synaptic gain with increasing light adaptation can be seen most clearly in the NLN model characteristics (Fig. 11), where there was a reduction in the slope of the first nonlinear system, as well as a reduction in the amplitude of the linear system.

DISCUSSION

Signal transmission in graded potential synapses is poorly understood in general, but this type of synapse is particularly well suited to the use of white noise nonlinear analysis techniques. Using the estimated output of the photoreceptor as an input to the synapse enabled us to characterize its dynamic nonlinear properties. Because all of the recordings were conducted under current-clamp conditions, the LMC responses may have included contributions from voltage-activated con-

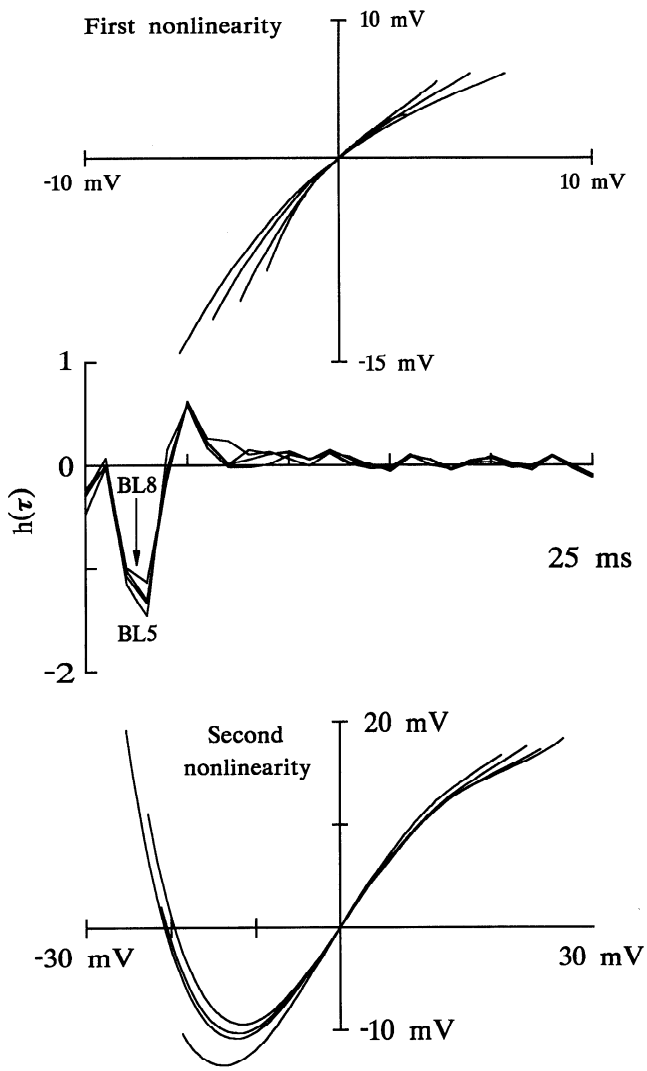

FIG. 11. Components of the NLN model at levels BL5–BL8. *Top*: 1st nonlinear static component. Amplitude range of the input signal increased with background level, so the shortest trace is from BL5, and the longest is from BL8. *Middle*: impulse response of the linear dynamic component. Note the similar time course of the response at all levels. *Bottom*: 2nd nonlinear static component. Lengths of the lines again correspond to the background levels, BL8 giving the longest trace.

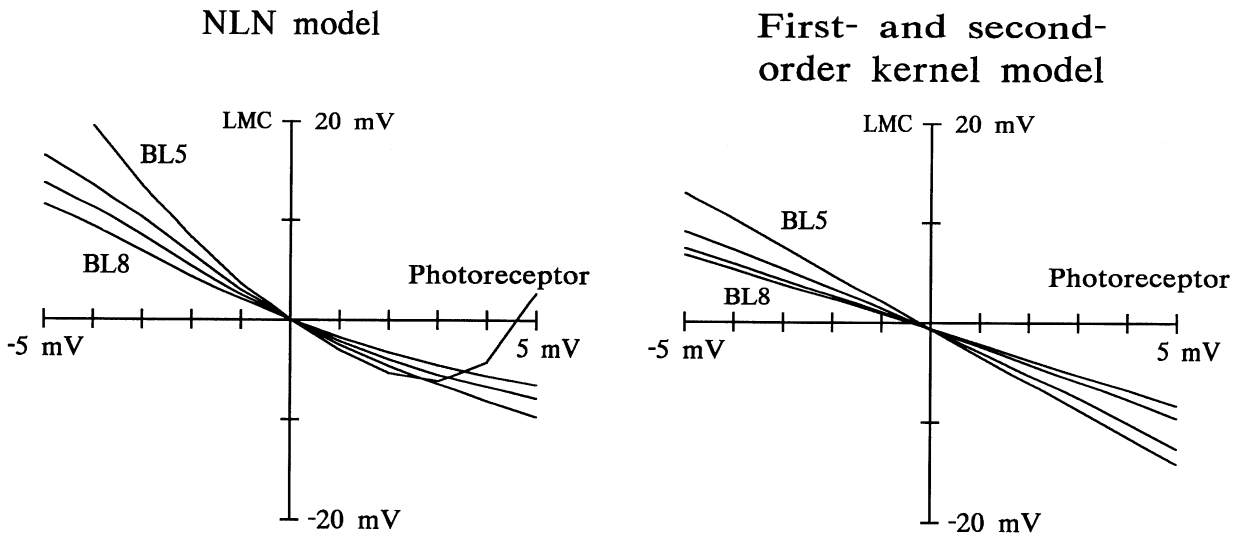

FIG. 12. Peak amplitudes of responses in the photoreceptor-LMC synapse when stimulated by a brief pulse in photoreceptor membrane potential, as predicted by the NLN model (*left*) and the 1st- and 2nd-order kernels (*right*) for levels BL5–BL8. Both models gave clear reductions in synaptic gain with increasing light adaptation.

ductances in the LMCs themselves. Therefore the measured synaptic function could include some local, postsynaptic effects. This broad definition of synaptic function has been widely used before in these systems. Voltage-clamp recordings may eventually be able to separate purely synaptic from local postsynaptic mechanisms.

The results show that two types of simple nonlinear models of the photoreceptor-LMC synapse are useful for describing its behavior over a wide range of background light intensities, whereas a LNL model was clearly not useful. We will discuss these results first in modeling terms and then suggest biological processes that could be responsible for the observed nonlinearities.

Model for synaptic transmission

The Volterra series of *Eq. 2* gave good fits to the data (MSE $< 10\%$) with only zero-order, first-order, and second-order kernels. The simplest physical model for such a series is to have two parallel pathways from input to output, the first passing through a purely linear system (k_1), and the other passing through a purely second-order system (k_2). However, the NLN cascade structure (Fig. 1) was also adequate to account for the data, with relatively low MSE levels. This second model, if accepted, would imply a simple flow-through structure, with different linear and nonlinear operations occurring at several stages of the synapse. The LNL cascade model was clearly unsuitable for fitting the data (Fig. 9). This also means that models that are subsets of the LNL structure, the Wiener and Hammerstein models, can be excluded.

This kind of modeling has been attempted before (James 1992), although at only one level of light adaptation. This earlier report also found that a LNL cascade could not account for the nonlinear behavior and suggested that modeling by parallel LNL structures might be useful. However, it is impossible to derive component parameters for such structures from the measured first- and second-order kernels.

Physical interpretation of the models, and changes induced by light adaptation

Are there any known physical processes that could correspond to the mathematical components of either of the two successful models? The obvious additional parallel pathway from the photoreceptor to the LMC is via the extracelluar space. During a light stimulus, the extracelluar space depolarizes by as much as 30 mV relative to ground. Other extracelluar effects could be due to changing ion composition, e.g., chloride concentration. These processes are relatively slow (Shaw 1984) but could contribute to light adaptational changes, by subtracting the low-frequency background from the signal in the presynaptic photoreceptor terminals (Juusola et al. 1995; Laughlin et al. 1987).

With increasing light adaptation, the presynaptic photoreceptors are increasingly depolarized. This may lead to increasing activation of the fast depolarizing transients (FDT) in the photoreceptor axons (Weckström et al. 1992). At the same time, the postsynaptic LMCs hyperpolarize (at least with moderate light adaptation) (Juusola et al. 1995), and the reversal potential for the transmitter-gated conductance, E_{Cl}, depolarizes (Uusitalo and Weckström 1994). These changes tend to decrease the gain in the synapse and restrict the amplitude of the postsynaptic signals. The processes changing synaptic function with light adaptation could decrease the linear gain but make the synapse more nonlinear.

The time courses of the synaptic second-order kernels (Fig. 8) are comparable with the linear synaptic function at each light background. Therefore any parallel mechanisms leading to the second-order kernels would need to be as fast as the chemical transmission. This probably rules out slow potential changes or chemical changes in the extracelluar space from playing a role in the measurements made here. It also makes it unlikely that any multisynaptic parallel pathway was involved.

For the NLN cascade model, either pre- or postsynaptic mechanisms could make major contributions to the components. The time courses of the synaptic kernels correspond

well to the light-off component of LMC impulse responses (Juusola et al. 1995). Previously, step responses in LMCs were divided into linear and nonlinear components, consisting of the (light-on) hyperpolarization and the (light-off) depolarization (Laughlin et al. 1987). The light-off response is partly caused by a voltage-activated sodium conductance (Uusitalo et al. 1995b). This "spiking" mechanism may be enhanced by light-induced hyperpolarization, due to a reduction of sodium channel inactivation. Such voltage dependence is an obvious nonlinearity, and the synaptic kernels displayed delayed depolarization spreading along the diagonal, suggesting that additional processes are triggered by the initial signal.

The linear part of the NLN model, $h(\tau)$, has properties that correspond well to signal transmission in a fast chemical synapse (e.g., Hardie 1989), where the transmitter release is tonic (Laughlin and Osorio 1989; Weckström et al. 1989; Uusitalo et al. 1995a) and can therefore be either increased or decreased. This would explain the biphasic nature of $h(\tau)$. Once released, the transmitter acts rapidly on the postsynaptic membrane. The half-life of transmitter-gated channels is ~0.5 ms (Hardie 1989), and the postsynaptic neurons have a membrane time constant of ~2 ms (Laughlin and Osorio 1989).

If $h(\tau)$ represents chemical transmission, the first nonlinear function of Fig. 11 would be produced by voltage changes in the photoreceptor axon terminal, or by the relationship between the voltage in the photoreceptor terminal and transmitter release. It has been shown that the rising phases of presynaptic contrast responses are enhanced by the FDT in photoreceptor axon terminals (Juusola et al. 1995; Weckström et al. 1992). The FDT channels are tuned to amplify and separate small contrast changes from the mean photoreceptor potential. In this scheme, the first static nonlinearity represents a modulation of the mean photoreceptor potential in the axon terminals, which drives voltage-sensitive transmitter release. This is further enhanced presynaptically by the FDT. The fact that both $h(\tau)$ and the synaptic gain (Fig. 11) decreased with increased light adaptation suggests a reduction in the sensitivity of transmitter release, possibly by inactivation of presynaptic calcium channels.

The final static nonlinearity of the NLN model might represent several different postsynaptic phenomena. Large hyperpolarizations could remove inactivation of a voltage-sensitive sodium conductance found in L1 and L3, and responsible for the so-called off-spike (Uusitalo et al. 1995b) and compress the subsequent responses. This would lead to the negative slope region at strong hyperpolarizations. The hyperpolarizing responses would also remove the inactivation of voltage-sensitive potassium channels in the postsynaptic membrane (Hardie and Weckström 1990; Uusitalo et al. 1995b). The steep midregion of the curve could be related to the kinetics of histamine-gated chloride channels, which have a steep dose dependence on transmitter concentration (Hardie 1989) because of high cooperativity.

Conclusions

The nonlinear models developed here provide relatively simple quantitative characterizations of synaptic transmission in the fly compound eye. The reduction in synaptic gain with light adaptation, as well as the nonlinear compression of LMC responses to large positive contrasts (negative membrane potential responses) agree with other experimental measurements and with linear analysis of the synapse (Juusola et al. 1995). The NLN model suggests that the reduction in gain occurs at relatively early stages of transmission, in the presynaptic photoreceptor axons and chemical transmission, whereas the nonlinear compression occurs relatively later, in the LMC membrane potential responses. All of the measurements support a picture of synaptic function in which the overall gain is reduced with increasing light adaptation.

We thank E. Kouvalainen for technical assistance and Prof. Juhani Leppäluoto for help and encouragement.

Support for this work was provided by the Academy of Finland, the Medical Research Council of Canada, the Oskar Öflund Foundation, the Emil Aaltonen Foundation, and the Finnish Medical Society Duodecium.

Address for reprint requests: A. S. French, Dept. of Physiology and Biophysics, Dalhousie University, Halifax, Novia Scotia B3H 4H7, Canada.

Received 17 April 1995; accepted in final form 25 July 1995.

REFERENCES

CHEN, H. W., ISHII, N., AND SUZUMURA, N. Structural classification of nonlinear systems by input and output measurements. *Int. J. Syst. Sci.* 17: 741–774, 1986.

DUBS, A. Non-linearity and light adaptation in the fly photoreceptor. *J. Comp. Physiol. A Sens. Neural Behav. Physiol.* 144: 53–59, 1981.

ECKERT, H. AND BISHOP, L. G. Nonlinear dynamic transfer characteristics of cells in the peripheral visual pathway of flies. *Biol. Cybern.* 17: 1–6, 1975.

FRENCH, A. S. Phototransduction in the fly compound eye exhibits temporal resonances and a pure time delay. *Nature Lond.* 283: 200–202, 1980a.

FRENCH, A. S. The linear dynamic properties of phototransduction in the fly compound eye. *J. Physiol. Lond.* 308: 385–401, 1980b.

FRENCH, A. S. AND JÄRVILEHTO, M. The dynamic behaviour of photoreceptor cells in the fly in response to random (white noise) stimulation at a range of temperatures. *J. Physiol. Lond.* 274: 311–322, 1978.

FRENCH, A. S., KORENBERG, M., JÄRVILEHTO, M., KOUVALAINEN, E., JUUSOLA, M., AND WECKSTRÖM, M. The dynamic nonlinear behaviour of fly photoreceptors evoked by a wide range of light intensities. *Biophys. J.* 65: 832–839, 1993.

FRENCH, A. S. AND KORENBERG, M. J. A nonlinear cascade model of action potential encoding in an insect sensory neuron. *Biophys. J.* 55: 655–661, 1989.

GEMPERLEIN, R. AND MCCANN, G. D. A study of the response properties of retinula cells of flies using nonlinear identification theory. *Biol. Cybern.* 19: 147–158, 1975.

HARDIE, R. C. A histamine-activated chloride channel involved in neurotransmission at a photoreceptor synapse. *Nature Lond.* 339: 704–706, 1989.

HARDIE, R. C. AND WECKSTRÖM, M. Three classes of potassium channels in large monopolar cells of the blowfly, *Calliphora vicina*. *J. Comp. Physiol. A Sens. Neural Behav. Physiol.* 167: 723–736, 1990.

VAN HATEREN, J. H. Neural superposition and oscillations in the eye of the blowfly. *J. Comp. Physiol. A Sens. Neural Behav. Physiol.* 161: 849–855, 1987.

VAN HATEREN, J. H. Theoretical predictions of spatiotemporal receptive fields of fly LMCs, and experimental validation. *J. Comp. Physiol. A Sens. Neural Behav. Physiol.* 171: 157–170, 1992.

HUNTER, I. W. AND KORENBERG, M. J. The identification of nonlinear biological systems: Wiener and Hammerstein cascade models. *Biol. Cybern.* 55: 135–144, 1986.

JAMES, A. C. Nonlinear operator network models of processing in the fly lamina. In: *Nonlinear Vision*, edited by R. Pinter and B. Nabet. Boca Raton, FL: CRC, 1992, p. 39–73.

JÄRVILEHTO, M. AND ZETTLER, F. Micro-localisation of lamina-located visual cell activities in the compound eye of blowfly *Calliphora*. *Z. Vergl. Physiol.* 69: 134–138, 1970.

JUUSOLA, M. Linear and nonlinear contrast coding in light adapted blowfly

photoreceptors. *J. Comp. Physiol. A Sens. Neural Behav. Physiol.* 172: 511–521, 1993.

JUUSOLA, M., KOUVALAINEN, E., JÄRVILEHTO, M., AND WECKSTRÖM, M. Contrast gain, signal-to-noise ratio and linearity in light-adapted blowfly photoreceptors. *J. Gen. Physiol.* 104: 593–621, 1994.

JUUSOLA, M., UUSITALO, R. O., AND WECKSTRÖM, M. Transfer of graded potentials at the photoreceptor-interneuron synapse. *J. Gen. Physiol.* 105: 117–148, 1995.

KIRSCHFELD, K. Die Projektion der optischen Umwelt auf das Raster der Rhabdomeren im Komplexauge von *Musca. Exp. Brain Res.* 3: 248–270, 1967.

KORENBERG, M. J. Identification of biological cascades of linear and static nonlinear systems. *Proc. Midwest Symp. Circuit Theory* 18.2: 1–9, 1973.

KORENBERG, M. J. Statistical identification of parallel cascades of linear and nonlinear systems. *I.F.A.C. Symp. Ident. Sys. Param. Est.* 1: 580–585, 1982.

KORENBERG, M. J. Identifying nonlinear difference equation and functional expansion representations: the fast orthogonal algorithm. *Ann. Biomed. Eng.* 16: 123–142, 1988.

KORENBERG, M. J. Parallel cascade identification and kernel estimation for nonlinear systems. *Ann. Biomed. Eng.* 19: 429–455, 1991.

KORENBERG, M. J., FRENCH, A. S., AND VOO, S. K. L. White noise analysis of nonlinear behavior in an insect sensory neuron: kernel and cascade approaches. *Biol. Cybern.* 58: 313–320, 1988.

KORENBERG, M. J. AND HUNTER, I. W. The identification of nonlinear biological systems: LNL cascade models. *Biol. Cybern.* 55: 125–134, 1986.

LAUGHLIN, S. B., HOWARD, J., AND BLAKESLEE, B. Synaptic limitations to contrast coding in the retina of the blowfly *Calliphora. Proc. R. Soc. Lond. B Biol. Sci.* 231: 437–467, 1987.

LAUGHLIN, S. B. AND OSORIO, D. Mechanisms for neural signal enhancement in the blowfly compound eye. *J. Exp. Biol.* 144: 113–146, 1989.

MARMARELIS, P. Z. AND MARMARELIS, V. Z. *Analysis of Physiological Systems. The White Noise Approach.* New York: Plenum, 1978.

MARMARELIS, V. Z. AND MCCANN, G. D. A family of quasi-white random signals and its optimal use in biological system identification. *Biol. Cybern.* 27: 57–62, 1977.

PRESS, W. H., FLANNERY, B. P., TEUKOLSKY, S. A., AND VETTERLING, W. T. *Numerical Recipes in C.* Cambridge, UK: Cambridge Univ. Press, 1990.

SHAW, S. R. Organization of the locust retina. *Symp. Zool. Soc. Lond.* 23: 135–163, 1968.

SHAW, S. R. Early visual processing in insects. *J. Exp. Biol.* 112: 225–251, 1984.

SRINIVASAN, M. V., PINTER, R. B., AND OSORIO, D. Matched filtering in the visual system of the fly: large monopolar cells of the lamina are optimized to detect moving edges and blobs. *Proc. R. Soc. Lond. B Biol. Sci.* 240: 279–293, 1990.

UUSITALO, R. O., JUUSOLA, M., KOUVALAINEN, E., AND WECKSTRÖM, M. Tonic transmitter release in a graded potential synapse. *J. Neurophysiol.* 74: 470–473, 1995a.

UUSITALO, R. O., JUUSOLA, M., AND WECKSTRÖM. M. Graded responses and spiking properties of identified first order visual interneurons of the fly compound eye. *J. Neurophysiol.* 73: 1782–1792, 1995b.

UUSITALO, R. O. AND WECKSTROM, M. The regulation of chloride homeostasis in the small nonspiking visual interneurons of the compound eye. *J. Neurophysiol.* 71: 1381–1389, 1994.

WECKSTRÖM, M., JUUSOLA, M., AND LAUGHLIN, S. B. Presynaptic enhancement of signal transients in photoreceptor terminals in the compound eye. *Proc. R. Soc. Lond. B Biol. Sci.* 250: 83–89, 1992.

WECKSTRÖM, M., JUUSOLA, M., UUSITALO, R., AND FRENCH, A. S. Fast-acting compressive and facilitatory nonlinearities in light-adapted fly photoreceptors. *Ann. Biomed. Eng.* 23: 70–77, 1995.

WECKSTRÖM, M., KOUVALAINEN, E., DJUPSUND, K., AND JÄRVILEHTO, M. More than one type of conductance is activated during responses of blowfly monopolar neurones. *J. Exp. Biol.* 144: 147–54, 1989.

WECKSTRÖM, M., KOUVALAINEN, E., AND JÄRVILEHTO, M. Non-linearities in response properties of insect visual cells: an analysis in time and frequency domains. *Acta Physiol. Scand.* 132: 103–113, 1988.